2DSBG: A 2d Semi Bi-Gaussian Filter Adapted for Adjacent and Multi-Scale Line Feature Detection

Baptiste Magnier, Ghulam Sakhi Shokouh, Louis Berthier, Marcel Pie, Adrien Ruggiero

2DSBG: A 2D SEMI BI-GAUSSIAN FILTER ADAPTED FOR ADJACENT AND MULTI-SCALE LINE FEATURE DETECTION

Baptiste Magnier, Ghulam Sakhi Shokouh, Louis Berthier, Marcel Pie and Adrien Ruggiero

EuroMov Digital Health in Motion, Univ Montpellier, IMT Mines Ales, Ales, France

ABSTRACT

Existing filtering techniques fail to precisely detect adjacent line features in multi-scale applications. In this paper, a new filter composed of a bi-Gaussian and a semi-Gaussian kernel is proposed, capable of highlighting complex linear structures such as ridges and valleys of different widths, with noise robustness. Experiments have been performed on a set of both synthetic and real images containing adjacent line features. The obtained results show the performance of the new technique in comparison to the main existing filtering methods.

***Index Terms*—** bi-Gaussian, semi-Gaussian, line features.

1. INTRODUCTION AND MOTIVATIONS

The detection of features in images is a computationally intensive process and remains a primary step in many low-level computer vision tasks. Linear structures (ridges, edges, etc.) are widely used features in various computer vision applications. To detect these linear structures, numerous filtering approaches have been implemented; originally, they were extracted by computing an impulse response of a simple line detector corresponding to a specific line/valley orientation (see [1], Eq.15.7-1). Incidentally, a review of line feature detection is presented in [2]. The optimal approach is chosen based on how to retain the maximum amount of desired information, whilst removing the noise to obtain an optimal segmentation result depending on the application. To that end, linear structure detection techniques require the analysis of the first or second order derivative of the images, which is obtained by filtering the image using a kernel convolution/correlation [3, 4, 5]. Gaussian kernels are the most popular and widely used filtering techniques due to their useful isotropy, steerability and decomposability properties related to the implementation of integration and differentiation in images [6, 7, 8]. The zeroth order Gaussian kernels $G(\sigma,x)=\frac{1}{\sqrt{2\pi}\sigma}\cdot \mathrm{e}^{-x^2/2\sigma^2}$ (with $\sigma\in\mathbb{R}_+^*$, $x\in\mathbb{R}$) are used for regularization [9]. The first and second order Gaussian kernels are commonly used for linear structure detection. However, these kernels are prone to noise, relative to both the derivative order and the σ parameter. Gaussian multi-scale is the primary method in scale-space feature analysis, as it let us with an option to keep good localization [10]. These techniques are mostly based on the eigen-decomposition of the Hessian matrix, as in [11, 10, 12, 2].

Meanwhile, steerable filters of second order (SF_2) are an elegant technique to capture ridge information; they are generated by the linear combination of basis filters [6] such as the second derivative of the Gaussian G'' in one dimension (1D):

$$G''(\sigma,x)=\frac{x^2-\sigma^2}{\sigma^4}\cdot \mathbf{e}^{\frac{-x^2}{2\cdot\sigma^2}},\ \text{with}\ \sigma\in\mathbb{R}_+^*,\ x\in\mathbb{R}. \qquad (1)$$

To improve the precision of the detection, elongated oriented filters were designed in terms of a better compromise between noise rejection and localization accuracy [13, 7, 14, 15], see isotropic versus anisotropic kernels in Fig. 1(a)-(b). Then, to extract line feature, the Second-Order Anisotropic Gaussian Kernel (SOAGK) can be applied in two dimensions (2D):

$$\text{SOAGK}\,(\sigma,\sigma_s,x,y)=\frac{x^2-\sigma^3}{2\pi\sigma^5\sigma_s}\mathrm{e}^{-\frac{1}{2}\left(\frac{x^2}{\sigma^2}+\frac{y^2}{\sigma_s^2}\right)},(\sigma,\sigma_s)\in\mathbb{R}_+^*\times\mathbb{R}_+^*. \qquad (2)$$

The choice of $\sigma_s>\sigma$ enables to build a narrow filter, then the filter is oriented to extract ridges, as illustrated in Fig. 1(b).

The second order Gaussian kernels are even kernels and the filter coefficients distant from the center of the filter have opposite signs. These even kernels get enlarged when the σ parameter is growing. Though this enlargement yields robustness against noise, the problem is that it unfavorably merges the adjacent lines (detailed in [15], Sec. 2 and Fig. 3). Therefore, an empirical trade-off when adjusting the parameter configuration (kernel support versus σ) is unavoidable in the conventional manner. In particular, adjacent and close linear structures of different widths cannot be accurately extracted with this type of filter. The proposed solution consists in seizing the properties of both a precisely orientable filter (Semi-Gaussian [16, 17]) and an adjustable filter under certain conditions of adjacent linear structures, see the different filters in Figs. 1(a)-(b). As a result, a new filter is generated, named 2D-Semi-Bi-Gaussian filter (2DSBG). The 2DSBG rigorously minimizes the interference of adjacent line features [18] while retaining adequate line feature information thanks to the fine-tuning of σ and the scale ratio parameter.

(a) SF_2 (b) SOAGK (c) SDSG (d) 2DSBG , ρ = 0.5

Fig. 1. 2D discrete filters of second order steered at 0° and 20°. For the derivative part G'' or BG'' in (d), $\sigma = 3.91$ whereas for (b)-(d), the anisotropic parameter $\sigma_s = 5\cdot\sigma$.

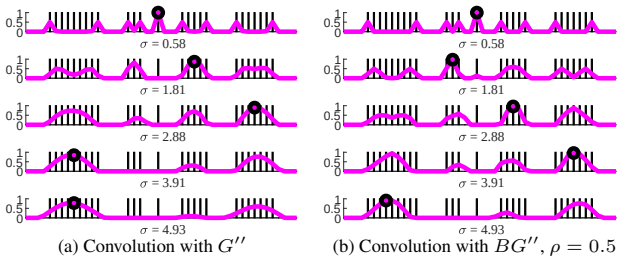

(a) Convolution with G'' (b) Convolution with BG'', $\rho = 0.5$

Fig. 2. Ridge highlighting in 1D for different scales σ. G'' and BG'' convolutions are used in (a) and (b) respectively. The blue bars represent the original signal containing separated ridges, while the convolved signals are plotted in orange and the maximum of each signal is displayed by black circles. As detailed in [2], σ values are tied to the optimum parameters for G'' as a function of the feature size from 1 to 9 pixels.

2. PROPOSED APPROACH: 2DSBG

The objective is to detect several line features in an image at different unknown positions, scales and orientations. By means of a truncation function, the detection procedure is formulated as a rotational matched filtering from 0 to 360°.

2.1. Prior Work: Bi-Gaussian Filter

The second order Gaussian G'' presented in Eq. (1) is useful to determine the location of linear structures [11, 10, 15, 17]. However, this simple Gaussian kernel relies on only one parameter to determine its shape: σ. This denotes one of the main well-known drawbacks of the Gaussian filter. Due to the length of its support, this is therefore not sufficient to differentiate between adjacent or closely related structures, especially when the σ value is large [18]. Consequently, linear structures cannot be suitably separately detected without any delocalization or fusion due to the regularization filter [19], as illustrated in Fig. 2(a). To address this drawback, the main idea is to transform the initial Gaussian filter into a bi-Gaussian, which combines the merits of the Gaussian and the Rectangular kernels. The benefits of this kernel are that it has a scale ratio able to clearly separate adjacent structures and, at the same time, the Gaussian part gives it robustness against noise. To tune the BG'' filter, a σ_b parameter allows us to play on the width and the sharpness of the curves on both sides of the central part [18]. To simplify, a parameter ρ is defined as the scale ratio: $\rho = \frac{\sigma_b}{\sigma}$. Hence, a ρ value ranging in $]0, 1]$ improves the detection of peaks, especially for adjacent contours, by making the bi-Gaussian kernel narrower. The influence of ρ value is studied in the next section. The second order bi-Gaussian filter BG'' is expressed as follows:

$$BG''(\sigma, \sigma_b, x) = \begin{cases} \rho^2 \cdot G''(\sigma_b, x - \sigma_b + \sigma) & \text{if } x \leq -\sigma \\ G''(\sigma, x) & \text{if } |x| < \sigma \\ \rho^2 \cdot G''(\sigma_b, x + \sigma_b - \sigma) & \text{if } x \geq \sigma. \end{cases} \quad (3)$$

When $\rho = 1$, the BG'' filter is equivalent to the 2nd derivative of the Gaussian G''. The Fig. 3 shows the 1D normalized BG'' filters for different values of σ and ρ. This filter's shape behaves in an opposite manner to Ziou's filter, which is very sharp in the middle, but contains the large length of its support

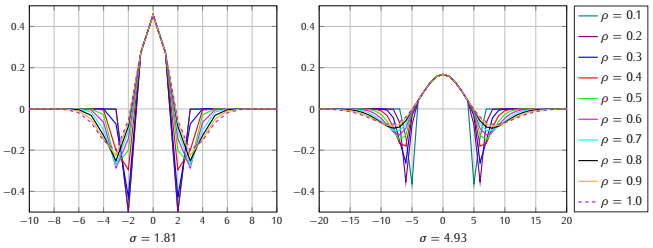

Fig. 3. Discrete second derivatives of bi-Gaussians in 1D computed using different parameters $\rho = \frac{\sigma_b}{\sigma}$. and see Eq. (3).

[20][2]. For the multi-scale step, the highest filtered value is retained along the different scales (see [2][17]). The Fig. 2(b) illustrates the application of the BG'' filter at different scales on a 1D signal containing different ridges of variable widths. The convolved signals are plotted, and the maximum of the signal is displayed where each ridge is tied to a specific scale (width of value 1, 3, 5, 7 and 9). Contrary to the Gaussian kernel in Fig. 2(a), the BG'' best fits the signal along the different scales, revealing the great interest of this filter shape.

2.2. Proposed Method: 2D Semi Bi-Gaussian Filter

The proposed technique (2DSBG) consists in combining a bi-Gaussian and a Semi-Anisotropic Gaussian filter which can be steered [21, 16, 17]. The main idea of the developed filter is to consider: (i) close and parallel neighboring ridges and linear feature and (ii) paths (i.e. ridges or valleys) crossing each pixel. To innovate, the proposed filter can detect close and parallel narrow bent ridges of different widths in two different directions thanks to the semi bi-Gaussian capacities.

It is inspired by the SDSG (Second-Derivative of a Semi-Gaussian [17]) where the main idea is to "*cut*" the SOAGK (Eq. (2)) using a Heaviside function and, then, steer this filter in all directions around the considered pixel: from 0 to 360° (steered by bilinear rotation, evaluated in [22]). Mathematically, the SDSG filter is defined by the combination of:

- a semi-Gaussian $\mathcal{G}$ for the smoothing, vertically truncated by a Heaviside function H, for $\sigma_s \in \mathbb{R}_+^*$ and $x \in \mathbb{R}$: $\mathcal{G}(\sigma_s, x) = H(x) \cdot \mathbf{e}^{-x^2/2 \cdot \sigma_s^2}$,
- a second derivative of a Gaussian G'' horizontally.

The proposed 2D filter substitutes the second order derivative of a Gaussian G'' for a second order derivative of a bi-Gaussian BG'' presented in Eq. (3): it is composed of Semi-Gaussian and bi-Gaussian operators. Note that for $\rho = 1$, the 2DSBG filter becomes the SDSG filter, see Fig. 1(c)-(d).

To adapt the multi-scale strategy, the response of the filter for different scaling parameters is configured - and the maximum value among the different filter responses can be selected [16]. When this new filter is steered towards the linear structure direction, the σ_s parameter allows an elongated smoothing in the line direction, whereas the σ captures the line structure strength (Eq. (3)). Then, the line structure strength is calculated using a local directional maximization/minimization (see [17]).

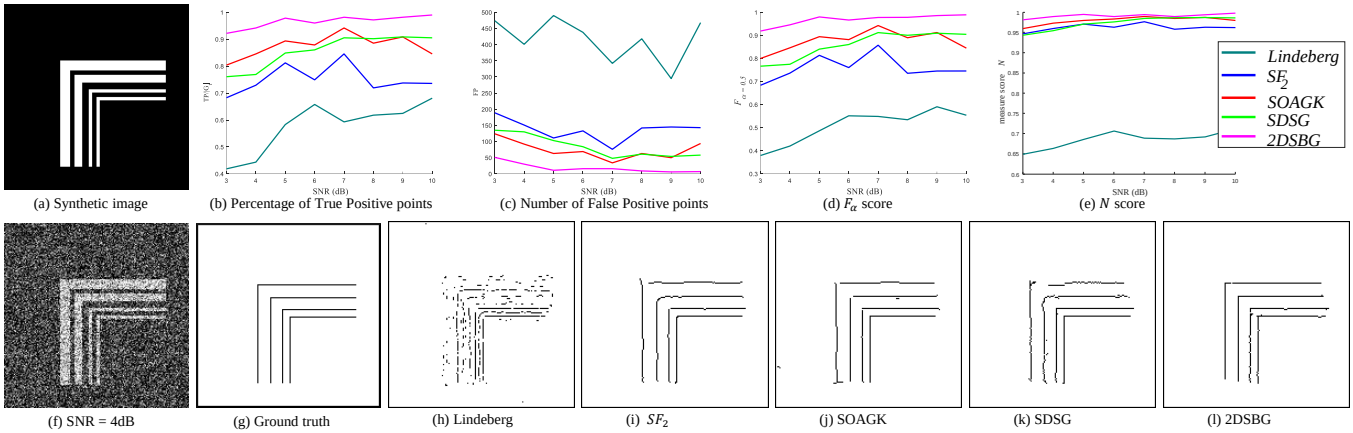

(a) Synthetic image (b) Percentage of True Positive points (c) Number of False Positive points (d) F_α score (e) N score

(f) SNR = 4dB (g) Ground truth (h) Lindeberg (i) SF_2 (j) SOAGK (k) SDSG (l) 2DSBG

Fig. 4. Evaluation of the ridge extraction techniques on synthetic images corrupted by a Gaussian noise between SNR=10dB and SNR=3dB ($\sigma_s = 5 \cdot \sigma$ for SOAGK, SDSG and 2DSBG). On the bottom: visualization of the best segmented images at SNR=4dB.

3. EXPERIMENTAL EVALUATION AND RESULTS

The proposed technique is evaluated on a set of both synthetic and real images-containing complex linear features such as close adjacent lines and ridges with varied scales. To evaluate the linear structure extraction, the *Normalized Figure of Merit* method [23] called $\mathcal{N}$ is employed. Thus, $\mathcal{N}$ calculates a standardized dissimilarity score; the closer the evaluation score is to 1, the more the linear structure is qualified as suitable. On the contrary, a score close to 0 corresponds with poor line feature detection, *i.e.* too much undesired detected pixels appear (false positives) or/and too many undetected points are missing (false negatives) in the detection result.

The aim here is to get the best contour map in a supervised way: theoretically, to be objectively compared, the ideal contour map must be the one for which the supervised evaluation $\mathcal{N}$ gets the highest score [23, 24]. In addition, from the proper binary confusion matrix, the precision (*Prec*) and *Recall* evaluations are computed, given the overall quality expressed in terms of the F_α-measure: $F_\alpha = \frac{Prec \cdot Recall}{\alpha \cdot Recall + (1-\alpha) \cdot Prec} = \frac{2TP}{2TP+FN+FP}$, when α=0.5, where *TP* represent true positive , *FP*: false positive and *FN*: false negative points respectively [24]. Also, $|G_t|$ represents the cardinality of true edges points in the ground truth map.

In this context, the 2DSBG filter is compared with 4 other multi-scale linear feature extraction techniques via filtering, namely: Lindeberg [10], SF_2 [6], SOAGK [15], and SDSG [17]. Evaluation scores for synthetic cases are presented in Figs. 4(b)-(e) for percentage of true positive ($TP/|G_t|$), false negative points, F_α and $\mathcal{N}$ measures respectively. In most cases, scores achieved by 2DSBG are superior to those of other techniques, showing the reliability of the proposed filter. Additionally, the Fig. 5 shows that the optimum parameter ρ for the 2DSBG belongs to $[0.5, 0.7]$ and its reliability increases when ρ<1, compared to the SDSG filter (corresponding to ρ = 1). Thus, the prominence of the proposed 2DSBG filter is confirmed in Fig. 4, where the Linderberg and SF_2 present the worst results with adjacent linear features because of their unadjustable kernel. The SDSG [17] obtains desirable results for the close and narrowly bent contours, but undesirable results in the case of wider contours due to the sensitivity of the second-order kernel. The SOAGK and 2DSBG produced broken lines when applied to thick and thin linear structures respectively. However, the fractures obtained with 2DSBG are very small and recoverable via post-processing.

Regarding real images, the 5 multi-scale linear feature extraction techniques are compared and evaluated together on the Ghent University Fungal Images 1 (GUFI-1) dataset which contains 100 images, extracted from fungi grown in vitro [15]. The resolution of images is 300×300 pixels, consist of hand-labelled ground truth data. Visually, the results presented in Fig. 6 indicate that Linderberg's method and especially the SF_2 produce erroneous contours and thus have a low segmentation quality. Although SDSG has been able to detect most of the contour details as well as the bent and narrow structures, it also generated erroneous points due to its second-order noise sensitivity. Accordingly with the previous performance results, the 2DSBG clearly extracts the most contours, especially in the case of narrow and adjacent lines,

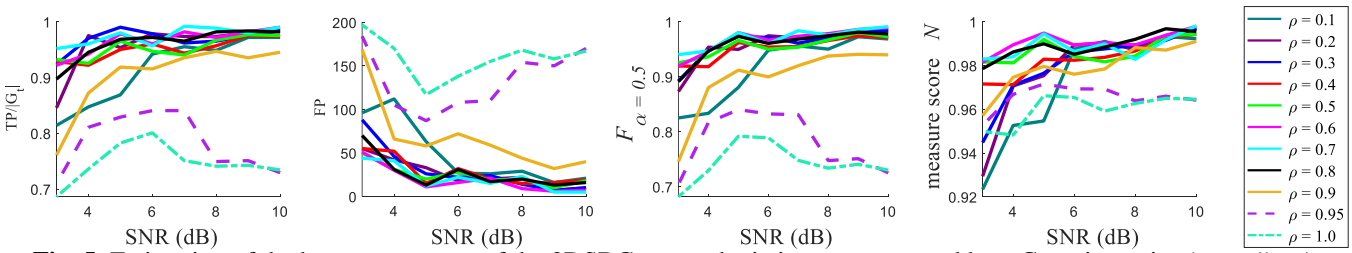

Fig. 5. Estimation of the best ρ parameter of the 2DSBG on synthetic images corrupted by a Gaussian noise ($\sigma_s = 5 \cdot \sigma$).

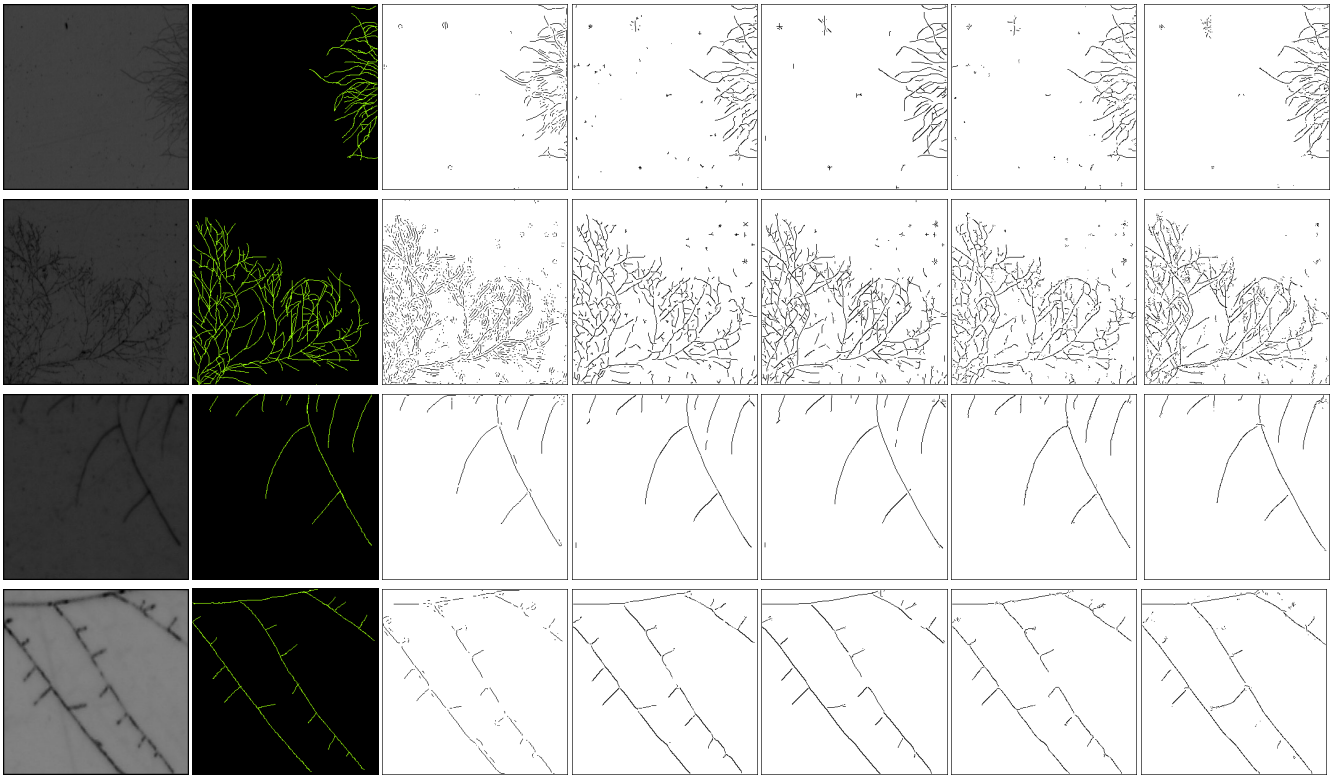

(a) Image 300×300 (b) Hand labelled (c) Lindeberg [10] (d) SF_2 [6] (e) SOAGK [15] (f) SDSG [17] (g) 2DSBG

Fig. 6. Images of size 300×300. Comparison of the proposed filter-2DSBG with the four state-of-the-art filters in the detection of linear structures in real fungus images. Parameters for SOAGK, SDSG and 2DSBG filters are the same: $\sigma_s = 5 \cdot \sigma$.

with barely any erroneous points.

Statistically, the 2DSBG filter is compared with four filtering based state-of-the-art techniques in scale-space, the scores are reported in the Tab. 1. As it is observed, the mean evaluation scores of F_α and $\mathcal{N}$ measures, achieved by the proposed filter are better to those of compared techniques, presenting the accuracy reliability of the 2DSBG filter.

4. DISCUSSION AND CONCLUSION

2DSBG, a new filter for multi-scale linear features extraction in images, constructed from bi-Gaussian and second-order semi-Gaussian filters is presented. This filter exploits the advantages of the bi-Gaussian for the detection of adjacent linear features, as well as the qualities presented by semi-Gaussian kernels for the analysis of bent and complex linear structures. Experiments on synthetic and real images were performed, allowing us to find the optimal parameter configuration ($\rho \in [0.5, 0.7]$), and thus confirming the novelty and merit of the 2DSBG over the existing filtering methods.

Table 1. Line feature detection performance of different methods on the dataset of 100 fungi images.

Method	Lindeberg [10]	SF_2 [6]	SOAGK [15]	SDSG [17]	2DSBG
$F_{\alpha=0.5}$	0.21	0.22	0.24	0.26	**0.29**
$\mathcal{N}$	0.72	0.75	0.77	0.78	**0.81**

To supplement this study, the contour detection models in deep learning generalize the contours and thus give the approximate structure whereas the proposed filter offers more accurate results especially for fine-grained ridges and noisy images. As an example, the result presented by the deep learning approach in [25] is different and does not have quite the context to compare with our proposed technique. The difference is that the deep learning based methods are trained to detect rather the generic low-level features (interest points, edges, ridges/valleys, corners, spots, etc.), and they usually do not extract a specific types of low-level features, such as if we want to extract only the contours of types of ridges/valleys. Additionally, if we aim to obtain a particular type of contour, it necessitates a large dataset with accurate and precise hand-labelled ground truth, we might be able to obtain comparable result (with lots of manual hyperparameter tuning to avoid over-fitting). However, based on our scope, no such types of dataset is available, because developing this type of dataset is quite error-prone and time-consuming process.

To conclude, the proposed filtering technique can be used as pre-processing, then be fed to Hough transform or neural network for enhancing specific object detection/classification tasks. For many tasks, classic filtering is used with the combination of neural network for optimizing the result, as in [26].

5. REFERENCES

[1] W Pratt and J Adams, "Digital Image Processing, 4th edition, J. Wiley & Sons," 2007.

[2] G.-S. Shokouh, B. Magnier, B. Xu, and P. Montesinos, "Ridge detection by image filtering techniques: A review and an objective analysis," *Pattern Recognition and Image Analysis: Advances in Mathematical Theory and Applications*, vol. 31, no. 3, pp. 551–570, 2021.

[3] D. Ziou and S. Tabbone, "Edge detection techniques: an overview," *International Journal on Pattern Recognition and Image Analysis*, vol. 8, no. 4, pp. 537–559, 1998.

[4] G. Papari and N. Petkov, "Edge and line oriented contour detection: State of the art," *IVC*, vol. 29, no. 2, pp. 79–103, 2011.

[5] P. Getreuer, "A survey of gaussian convolution algorithms," *Image Processing On Line*, vol. 2013, pp. 286–310, 2013.

[6] W.T. Freeman and E. H. Adelson, "The design and use of steerable filters," *IEEE TPAMI*, vol. 13, no. 9, pp. 891–906, 1991.

[7] M. Jacob and M. Unser, "Design of steerable filters for feature detection using canny-like criteria," *IEEE TPAMI*, vol. 26, no. 8, pp. 1007–1019, 2004.

[8] G. Papari, P. Campisi, and N. Petkov, "Steerable filtering using novel circular harmonic functions with application to edge detection," in *IEEE ICPR*, 2010, pp. 3947–3950.

[9] J. Canny, "A computational approach to edge detection," *IEEE TPAMI*, pp. 679–698, 1986.

[10] T. Lindeberg, "Edge detection and ridge detection with automatic scale selection," *Int. J. of Comput. Vis.*, vol. 30, no. 2, pp. 117–156, 1998.

[11] C. Steger, "An unbiased detector of curvilinear structures," *IEEE TPAMI*, vol. 20, no. 2, pp. 113–125, 1998.

[12] B. Tremblais, A.S. Capelle-Laize, and B. Augereau, "Algorithms for the extraction of various diameter vessels," *Cellular and Molecular Biology*, vol. 53, no. 2, pp. 62–74, 2007.

[13] P. Perona, "Steerable-scalable kernels for edge detection and junction analysis," *IVC.*, vol. 10, no. 10, pp. 663–672, 1992.

[14] P. Arbelaez, M. Maire, C. Fowlkes, and J. Malik, "Contour detection and hierarchical image segmentation," *IEEE TPAMI*, vol. 33, no. 5, pp. 898–916, 2010.

[15] C. Lopez-Molina, G. Vidal-Diez de Ulzurrun, J.M. Baetens, J. Van den Bulcke, and B. De Baets, "Unsupervised ridge detection using second order anisotropic gaussian kernels," *Signal Processing*, vol. 116, pp. 55–67, 2015.

[16] B. Magnier, A. Aberkane, P. Borianne, P. Montesinos, and C. Jourdan, "Multi-scale crest line extraction based on half gaussian kernels," in *IEEE ICASSP*, 2014, pp. 5105–5109.

[17] B. Magnier, G.-S. Shokouh, B. Xu, and P. Montesinos, "A multi-scale line feature detection using second order semi-gaussian filters," in *CAIP*. 2021, vol. 13053 of *LNCS*, pp. 98–108, Springer International Publishing.

[18] C. Xiao, M. Staring, Y. Wang, Shamonin D. P., and B. C. Stoel, "Multiscale bi-gaussian filter for adjacent curvilinear structures detection with application to vasculature images," *IEEE TIP*, vol. 22, pp. 174–188, 2013.

[19] O. Laligant, F. Truchetet, and F. Meriaudeau, "Regularization preserving localization of close edges," *IEEE Signal Processing Letters*, vol. 14, no. 3, pp. 185–188, 2007.

[20] D. Ziou, "Optimal line detector," in *ICPR*, 2000, vol. 3, pp. 530–533 vol.3.

[21] B. Magnier, D. Diep, and P Montesinos, "Perceptual curve extraction," in *IEEE IVMSP Workshop: Perception and Visual Signal Analysis*. IEEE, 2011, pp. 93–98.

[22] B. Magnier, B. Moradi, and P. Carré, "Evaluation of half gaussian filter rotation for edge detection," in *EUVIP*. IEEE, 2019, pp. 52–57.

[23] B. Magnier, "Edge detection evaluation: A new normalized figure of merit," in *IEEE ICASSP*, 2019, pp. 2407–2411.

[24] B. Magnier, H. Abdulrahman, and P. Montesinos, "A review of supervised edge detection evaluation methods and an objective comparison of filtering gradient computations using hysteresis thresholds," *Journal of Imaging*, vol. 4, no. 6, pp. 74, 2018.

[25] X. Soria, E. Riba, and A. Sappa, "Dense extreme inception network: Towards a robust CNN model for edge detection," in *IEEE WACV*, 2020, pp. 1912–1921.

[26] F. Cervantes-Sanchez, I. Cruz-Aceves, A. Hernandez-Aguirre, M. A. Hernandez-Gonzalez, and S. E. Solorio-Meza, "Automatic segmentation of coronary arteries in x-ray angiograms using multiscale analysis and artificial neural networks," *Applied Sciences*, vol. 9, no. 24, 2019.

2DSBG: A 2D SEMI BI-GAUSSIAN FILTER ADAPTED FOR ADJACENT AND MULTI-SCALE LINE FEATURE DETECTION

IMT Mines Alès
École Mines-Télécom

baptiste.magnier@mines-ales.fr

ICASSP 2023

ICASSP 2023
IEEE Signal Processing Society

Authors

Baptiste Magnier,
Ghulam-Sakhi Shokouh,
Louis Berthier,
Marcel Pie-Tapia,
Adrien Ruggiero

EuroMov Digital Health in Motion, Univ. Montpellier, IMT Mines Ales, Ales, France

CERIS, 6. avenue de Clavières 30100 Alès, France

Refrences:

[1] W Pratt and J Adams, "Digital Image Processing, 4th ed,, J. Wiley & Sons," 2007.
[2] G.-S. Shokouh, B. Magnier, B. Xu, and P. Montesinos, "Ridge detection by image filtering techniques: A review and an objective analysis," *PRIA*, 2021.
[3] D. Ziou and S. Tabbone, "Edge detection techniques: an overview," *IJPRIA*, 1998.
[4] G. Papari and N. Petkov, "Edge and line oriented contour detection: State of the art," *IVC*, 2011.
[5] P. Getreuer, "A survey of gaussian convolution algorithms," *IPOL*, 2013.
[6] W.T. Freeman and E. H. Adelson, "The design and use of steerable filters," *IEEE TPAMI*, 1991.
[7] M. Jacob and M. Unser, "Design of steerable filters for feature detection using canny-like criteria," *IEEE TPAMI*, 2004.
[8] G. Papari, P. Campisi, and N. Petkov, "Steerable filtering using novel circular harmonic functions with application to edge detection," in *IEEE ICPR*, 2010,
[9] J. Canny, "A computational approach to edge detection," *IEEE TPAMI*, 1986.
[10] T. Lindeberg, "Edge detection and ridge detection with automatic scale selection," *Int. J. of Comput. Vis.*, 1998.
[11] C. Steger, "An unbiased detector of curvilinear structures," *IEEE TPAMI*, 1998.
[12] B. Tremblais, A.S. Capelle-Laize, and B. Augereau, "Algorithms for the extraction of various diameter vessels," *Cellular and Molecular Biology*, 2007.
[13] P. Perona, "Steerable-scalable kernels for edge detection and junction analysis," *IVC*, 1992.
[14] P. Arbelaez, M. Maire, C. Fowlkes, and J. Malik, "Contour detection and hierarchical image segmentation," *IEEE TPAMI*, 2010.
[15] C. Lopez-Molina, G. Vidal-Diez de Ulzurrun, J.M. Baetens, J. Van den Bulcke, and B. De Baets, "Unsupervised ridge detection using second order anisotropic gaussian kernels," *Signal Processing*, 2015.
[16] B. Magnier, A. Aberkane, P. Borianne, P. Montesinos, and C. Jourdan, "Multi-scale crest line extraction based on half gaussian kernels," in *IEEE ICASSP*, 2014,
[17] B. Magnier, G.-S. Shokouh, B. Xu, and P. Montesinos, "A multi-scale line feature detection using second order semi-gaussian filters," in *CAIP*. 2021,
[18] C. Xiao, M. Staring, Y. Wang, Shamonin D. P., and B. C. Stoel, "Multiscale bi-gaussian filter for adjacent curvilinear structures detection with application to vasculature images," *IEEE TIP*, 2013.
[19] D. Ziou, "Optimal line detector," in *ICPR*, 2000.
[20] B. Magnier, D. Diep, and P Montesinos, "Perceptual curve extraction," in *IEEE IVMSP*, 2011.
[21] B. Magnier, B. Moradi, and P. Carre, "Evaluation of half ´ gaussian filter rotation for edge detection," in *EUVIP*. IEEE, 2019,
[22] B. Magnier, "Edge detection evaluation: A new normalized figure of merit," in *IEEE ICASSP*, 2019.
[23] B. Magnier, H. Abdulrahman, and P. Montesinos, "A review of supervised edge detection evaluation methods and an objective comparison of filtering gradient computations using hysteresis thresholds," *Journal of Imaging*, 2018.

I - Related Works

Type of edges: [3, 4, 9]

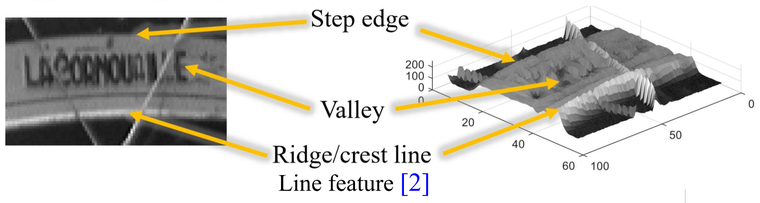

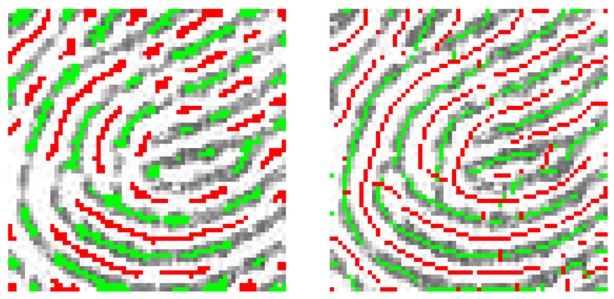

Ridges/valleys extracted by Laplacian of Gaussian.

Ridges/valleys extracted with the Hessian matrix.

Line feature detectors: Hessian matrix (eigenvalues) [2, 10, 11, 12]

$$\mathcal{H}(x,y) = \begin{pmatrix} I_{xx}(x,y) & I_{xy}(x,y) \\ I_{xy}(x,y) & I_{yy}(x,y) \end{pmatrix}$$

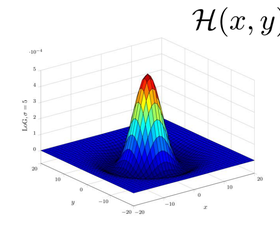

Laplacian/DOLP [2]

$$\begin{pmatrix} -1 & 2 & -1 \\ -2 & 4 & -2 \\ -1 & 2 & -1 \end{pmatrix}$$ Rotation

Line detector [1]

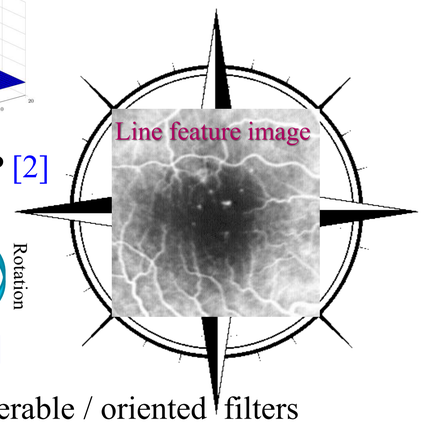

Steerable / oriented filters

(a) SF_2 [6, 8] (b) SOAGK [13, 14 ,15] (c) SDSG [16, 17 ,20]

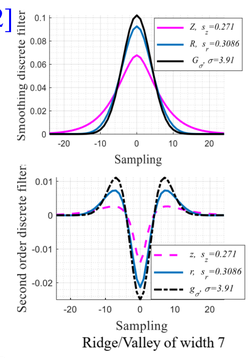

[19]	[2]	[2]
width	s_z	s_r	σ
1	1.696	2.05	0.58
3	0.63	0.69	1.81
5	0.37	0.42	2.88
7	0.27	0.31	3.91
9	0.21	0.24	4.93
11	0.17	0.20	5.94
13	0.15	0.17	6.95
15	0.13	0.15	7.95
17	0.12	0.13	8.96

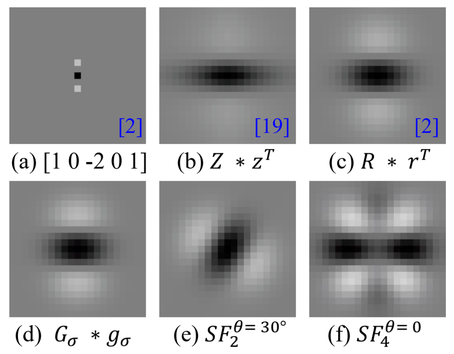

II – Proposed Approach: 2DSBG

2nd derivative of a bi-Gaussian filter (1D) [18]:

$$BG''(\sigma,\sigma_b,x) = \begin{cases} \rho^2 \cdot G''(\sigma_b, x-\sigma_b+\sigma) & \text{if } x \le -\sigma \\ G''(\sigma,x) & \text{if } |x| < \sigma \\ \rho^2 \cdot G''(\sigma_b, x+\sigma_b-\sigma) & \text{if } x \ge \sigma. \end{cases}$$

With $\rho = {}^{\sigma_b}/_{\sigma}$; if $\rho = 1$, $BG'' = G''$

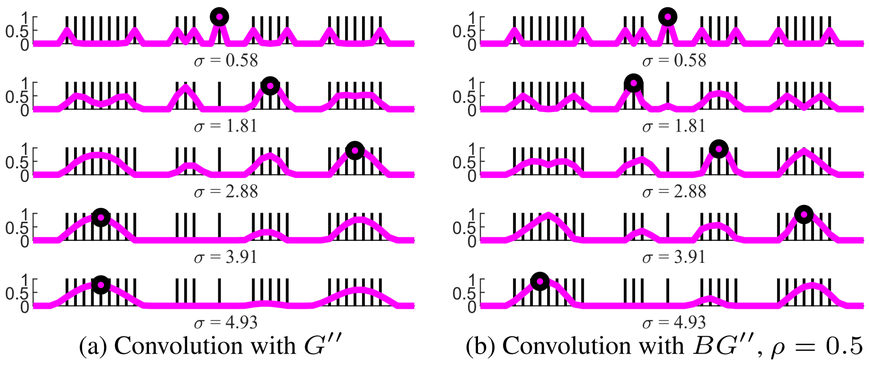

(a) Convolution with G'' (b) Convolution with BG'', $\rho = 0.5$

2nd derivative of a Gaussian filter (1D) $G''(\sigma,x) = \dfrac{x^2-\sigma^2}{\sigma^4} \cdot e^{\frac{-x^2}{2\cdot\sigma^2}}$, with $\sigma \in \mathbb{R}_+^*$, $x \in \mathbb{R}$.
if $\rho = 1$, $BG'' = G''$ (and $BG = G$)

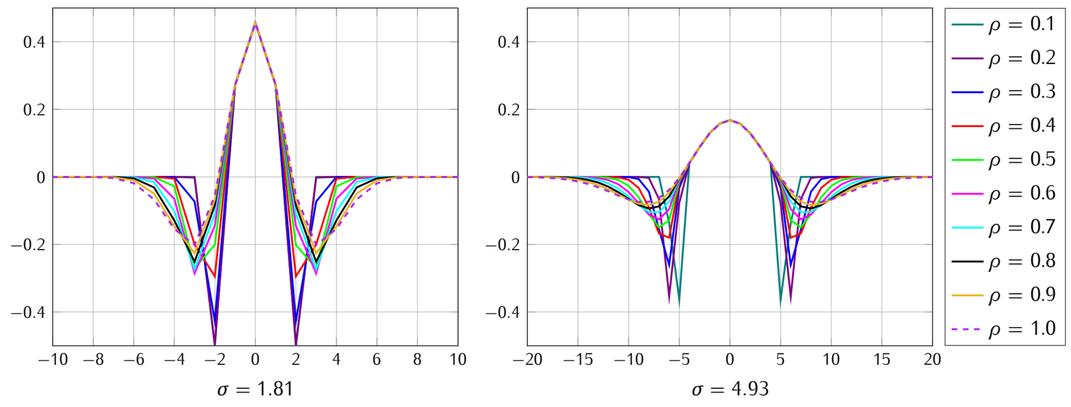

Mathematically, the 2DSBG filter is defined by the combination of:
• a semi-Gaussian for the smoothing, vertically truncated by a Heaviside function H :

$$\mathcal{G}(\sigma_s,x) = H(x) \cdot e^{-\frac{x^2}{2\sigma_s^2}}$$

• a second derivative of a bi-Gaussian BG'' horizontally,
then, steer this filter in all directions around the considered pixel: from 0 to 360° (steered by bilinear rotation, evaluated in [21]).

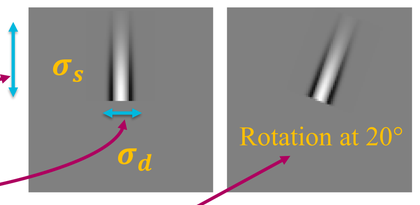

$\rho = 1$,
$2DSBG = SDSG$
[16, 17 ,20]

for reliability:
$\rho \in [0{,}5; 0{,}7]$,
and $\sigma_s \approx 5 \cdot \sigma_d$

III – Evaluation and Results

Normalized edge detection evaluation (involving distances of pixels) [22]:

$$\mathcal{N}(G_t,D_c) = \frac{1}{FP+FN} \cdot \left[\frac{FP}{|D_c|} \cdot \sum_{p \in D_c} \frac{1}{1+\delta \cdot d_{G_t}^2(p)} + \frac{FN}{|G_t|} \cdot \sum_{p \in G_t} \frac{1}{1+\kappa \cdot d_{D_c}^2(p)} \right]$$

Edge detection evaluation (pixel per pixel) [23]:

$$F_\alpha = \frac{\mathrm{P_{rec}} \cdot \mathrm{R_{ec}}}{\alpha \mathrm{P_{rec}} + (1-\alpha)\mathrm{R_{ec}}} \text{ with } \mathrm{P_{rec}} = \frac{TP}{TP+FP} \text{ and } \mathrm{R_{ec}} = \frac{TP}{TP+FN},$$

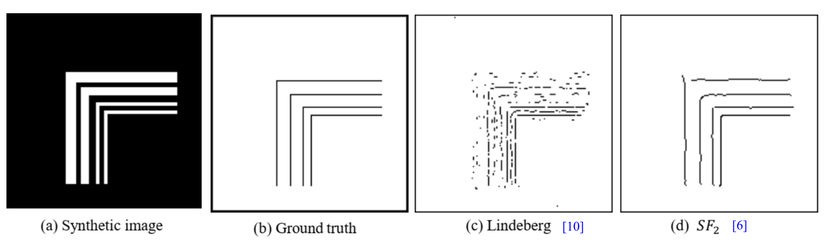

(a) Synthetic image (b) Ground truth (c) Lindeberg [10] (d) SF_2 [6]

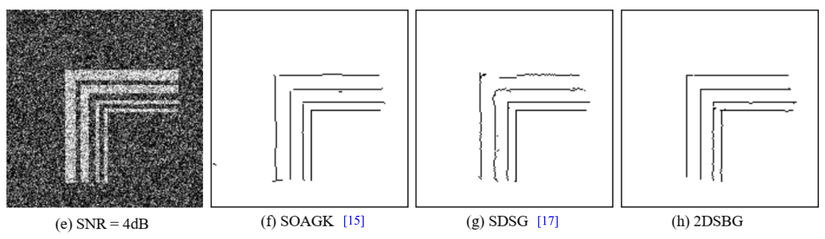

(e) SNR = 4dB (f) SOAGK [15] (g) SDSG [17] (h) 2DSBG

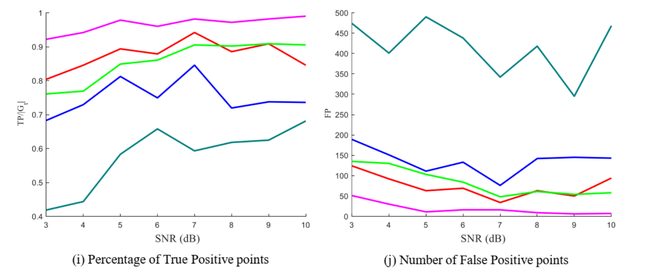

(i) Percentage of True Positive points (j) Number of False Positive points

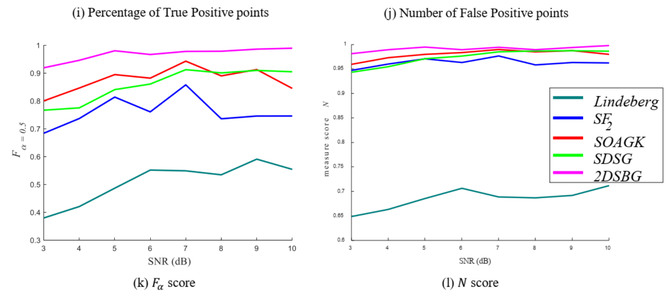

(k) F_α score (l) N score

Real images: Ghent University Fungal Images 1 (GUFI-1) dataset [15]

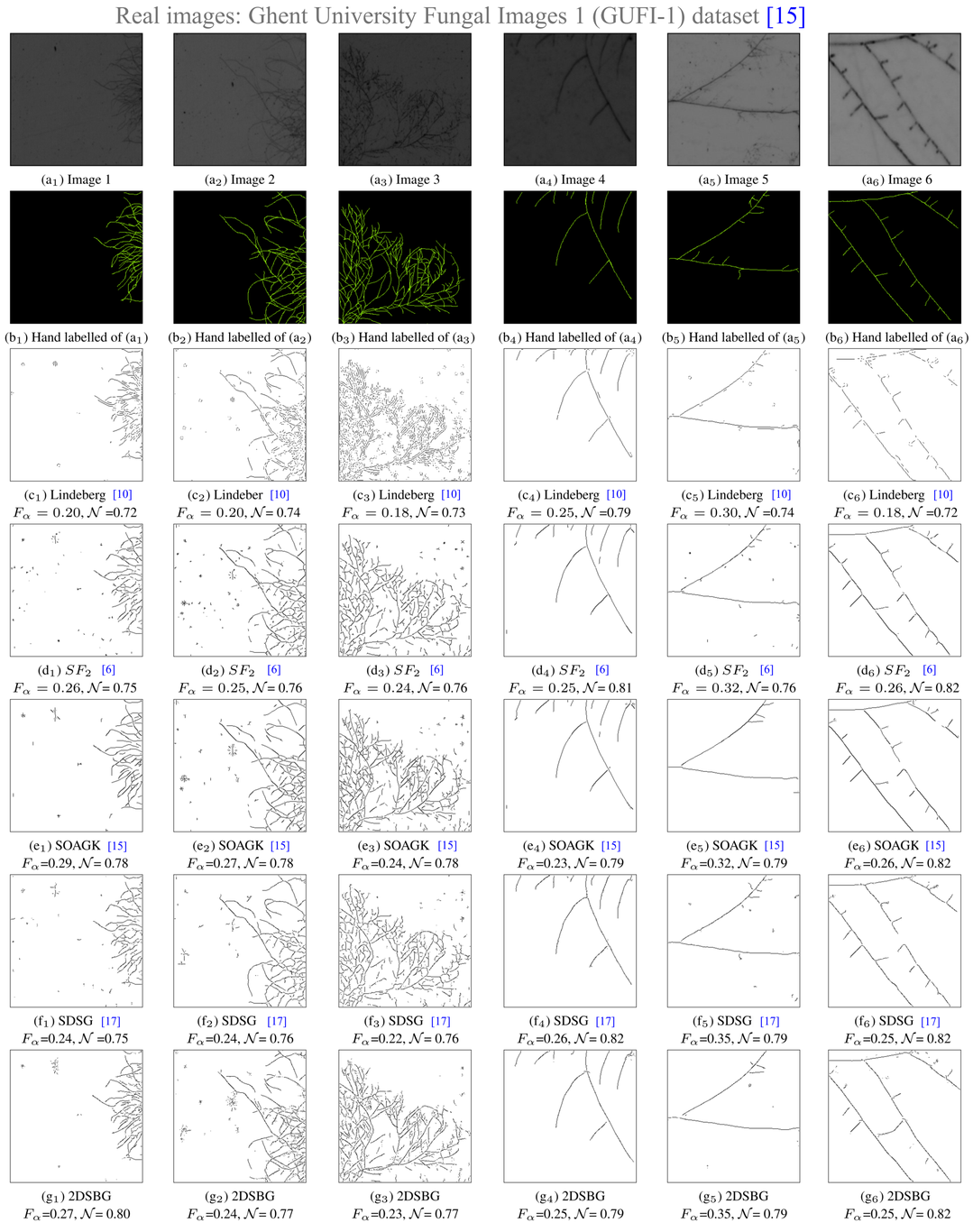

(a1) Image 1 (a2) Image 2 (a3) Image 3 (a4) Image 4 (a5) Image 5 (a6) Image 6
(b1) Hand labelled of (a1) (b2) Hand labelled of (a2) (b3) Hand labelled of (a3) (b4) Hand labelled of (a4) (b5) Hand labelled of (a5) (b6) Hand labelled of (a6)
(c1) Lindeberg [10] $F_\alpha = 0.20, \mathcal{N} = 0.72$ (c2) Lindeber [10] $F_\alpha = 0.20, \mathcal{N} = 0.74$ (c3) Lindeberg [10] $F_\alpha = 0.18, \mathcal{N} = 0.73$ (c4) Lindeberg [10] $F_\alpha = 0.25, \mathcal{N} = 0.79$ (c5) Lindeberg [10] $F_\alpha = 0.30, \mathcal{N} = 0.74$ (c6) Lindeberg [10] $F_\alpha = 0.18, \mathcal{N} = 0.72$
(d1) SF_2 [6] $F_\alpha = 0.26, \mathcal{N} = 0.75$ (d2) SF_2 [6] $F_\alpha = 0.25, \mathcal{N} = 0.76$ (d3) SF_2 [6] $F_\alpha = 0.24, \mathcal{N} = 0.76$ (d4) SF_2 [6] $F_\alpha = 0.25, \mathcal{N} = 0.81$ (d5) SF_2 [6] $F_\alpha = 0.32, \mathcal{N} = 0.76$ (d6) SF_2 [6] $F_\alpha = 0.26, \mathcal{N} = 0.82$
(e1) SOAGK [15] $F_\alpha = 0.29, \mathcal{N} = 0.78$ (e2) SOAGK [15] $F_\alpha = 0.27, \mathcal{N} = 0.78$ (e3) SOAGK [15] $F_\alpha = 0.24, \mathcal{N} = 0.78$ (e4) SOAGK [15] $F_\alpha = 0.23, \mathcal{N} = 0.79$ (e5) SOAGK [15] $F_\alpha = 0.32, \mathcal{N} = 0.79$ (e6) SOAGK [15] $F_\alpha = 0.26, \mathcal{N} = 0.82$
(f1) SDSG [17] $F_\alpha = 0.24, \mathcal{N} = 0.75$ (f2) SDSG [17] $F_\alpha = 0.24, \mathcal{N} = 0.76$ (f3) SDSG [17] $F_\alpha = 0.22, \mathcal{N} = 0.76$ (f4) SDSG [17] $F_\alpha = 0.26, \mathcal{N} = 0.82$ (f5) SDSG [17] $F_\alpha = 0.35, \mathcal{N} = 0.79$ (f6) SDSG [17] $F_\alpha = 0.25, \mathcal{N} = 0.82$
(g1) 2DSBG $F_\alpha = 0.27, \mathcal{N} = 0.80$ (g2) 2DSBG $F_\alpha = 0.24, \mathcal{N} = 0.77$ (g3) 2DSBG $F_\alpha = 0.23, \mathcal{N} = 0.77$ (g4) 2DSBG $F_\alpha = 0.25, \mathcal{N} = 0.79$ (g5) 2DSBG $F_\alpha = 0.35, \mathcal{N} = 0.79$ (g6) 2DSBG $F_\alpha = 0.25, \mathcal{N} = 0.82$